mater.scichina.com link.springer.com

Published online 28 April 2020 | https://doi.org/10.1007/s40843-020-1316-1
Sci China Mater 2020, 63(7): 1337–1344

Cu-doped CoS_2 polyhedrons with high catalytic activity and long-term stability

Jie Yin[1†], Pin Chen[2†], Minglong Lu[1†], Lili Song[1], Renyun Zhang[3], Feng Xu[4], Ningning Wu[2] and Yuqiao Wang[1*]

Transition metal sulfides are of great relevance in photoelectrochemical catalytic reactions [1–3], due to their unique electronic structure, tunable composition and morphology, and the possibility of large scale synthesis. We have been looking for low-cost, high-efficiency, and durable catalysts, and also aim to understand their catalytic mechanism and achieve their large-scale preparation. Currently, the main strategies toward these goals include: (1) a noble metal catalyst is replaced by non-precious metals, (2) the catalytic properties are regulated by surface engineering and heteroatom doping, (3) the catalytic mechanism is investigated by dynamics and thermodynamics. In previous studies, we have reported a number of highly efficient catalysts based on non-precious metals with specifically designed structures, such as coaxially layer-tunable MoS_2 [4], vertically edge-terminated MoS_2 [5], micropolyhedral ZnS [6,7], and heterojunction WS_2/MoS_2 [8]. The preparation methods include pulsed laser deposition, and hydrothermal and dipping methods combined with chemical vapor deposition.

These studies can be considered as starting points for proposing an innovative method to design and achieve highly efficient and stable catalysts. The development of such novel methods often implicate surface engineering [9–11] and organic/inorganic hybrid materials [12,13]; however, few studies have been successful. Enhancing the catalytic effect usually involves four aspects: (1) maximizing the specific surface area to increase the contact with the reactants; (2) tuning the electronic structure, adjusting the energy level and controlling the charge transfer efficiency by doping with hetero atoms; (3) directly exposing the highly active facets of a material by controlling the crystal growth process; (4) achieving a long lifetime based on the design of the physicochemical structure.

Cobalt sulfide is a widespread mineral that presents different stoichiometries, e.g., CoS, CoS_2, Co_3S_4, and Co_9S_8 [14]. Among them, cobalt pyrite (CoS_2) is considered a promising catalyst in the energy conversion and storage fields [15] because of its high electrocatalytic activity and cost-effectiveness. Numerous efforts have been made toward the surface engineering of CoS_2, since the electrocatalytic performance heavily relies on the surface area, atomic structure, morphology, and type of facet. These factors influence the catalytic activity and lifetime of the material, suggesting that it is of great importance to understand the relationship between the structure design, preparation method, and catalyst performance. For instance, NiS_2 octahedral nanocrystals with exposed (111) facets exhibit a higher catalytic performance toward I_3^- reduction than the cubic nanocrystals with (100) facets due to the better surface adsorption energy in the former [16]. Moreover, incorporating Fe ions into NiS_2 can effectively increase the adsorption energy of the iodine atom on the {111} facet to accelerate the reduction of I_3^- [17]. This means that doping may further improve the catalytic activity because dopants may affect the activity and stability of crystal planes. In addition, CoS_2 doped with P and N remarkably decreases the over-potentials for hydrogen evolution reactions because the reaction barriers decrease after doping [18,19]. Therefore, doping engineering may improve the activity and stability of active facets.

Herein, we designed Cu-doped CoS_2 polyhedrons that

[1] Institute of Advanced Materials, School of Chemistry and Chemical Engineering, Southeast University, Nanjing 211189, China
[2] National Supercomputer Center in Guangzhou (NSCC-GZ), Sun Yat-sen University, Guangzhou 510006, China
[3] Department of Natural Sciences, Mid Sweden University, Holmgatan 10, SE, 85170, Sundsvall, Sweden
[4] SEU-FEI Nano-Pico Center, Key Laboratory of MEMS of Ministry of Education, Southeast University, Nanjing, 210096, China
† These authors contributed equally to this work.
* Corresponding author (email: yqwang@seu.edu.cn)

contain {111}, {110}, and {100} planes. Their electronic structures, surface energies and surface adsorption energies before and after copper doping were predicted by first principle calculations. The polyhedrons were prepared on F-doped tin oxide (FTO) substrates by a hydrothermal method. The truncated tetragonal bipyramidal shape of CoS_2 can be transformed from octahedrons to polyhedrons after Cu doping. The growth mechanism of the polyhedrons was elucidated using a slab model and the Wulff construction. The catalytic efficiency and stability were estimated for the reduction reaction of I_3^- to I^-.

Density functional theory (DFT) calculations were performed to determine the electronic structure of CoS_2 before and after Cu doping in terms of the band structure and the partial and total density of states (PDOS and TDOS) analysis (Fig. 1a). CoS_2 is a typical n-semiconductor that shows metallic nature due to its d-electron configuration, $(t_{2g})^6(e_g)^1$ [20]. After Cu doping, no additional band gaps appear around the Fermi energy level, indicating the metallic nature of Cu-doped CoS_2. This is mainly because of the similarities between cobalt and copper, especially their atomic sizes, electronegativities, and bonding properties. The PDOS diagrams show two new energy bands near the Fermi level of Cu-doped CoS_2. This is caused by p-d hybridization, which results from the overlaps of S 3p orbitals with Co and Cu 3d orbitals. That is, there is a bonding effect on S–Co and S–Cu bonds. The major contributions on the TDOS near the Fermi levels are attributed to localized Co and Cu 3d orbitals. Therefore, the intrinsic metallicity, overlapped orbitals, and bonding effect would ensure a highly efficient electron transfer between reactants and catalysts, and thus promote the electrocatalytic efficiency.

For the catalytic kinetic model, the rate-determining step of the total reaction: $I_3^- + 2e^- \leftrightarrow 3I^-$, is the adsorption and desorption process between the iodine atom and the catalyst surface active site: $I_2 + 2e^- \leftrightarrow 2I^-$ [21]. The adsorption energy is employed to differentiate the interaction intensity between the catalyst surface and the electroactive species. The adsorption-desorption model between iodine and various crystal planes, such as the (111), (110), and (100) facets, was based on slab models (Fig. 1b). The adsorption energies between CoS_2 and the iodine atom are −3.49, 0.68 and −4.25 eV, for the (111), (110) and (100) facets. After Cu doping, the adsorption energy on these facets is −2.00, −1.52 and −3.13 eV, respectively. As a reference, the noble metal catalyst Pt has an adsorption energy of −1.26 eV [21]. This value allows to reach the equilibrium state during the adsorption and desorption processes. Before doping, the contribution of the (111) plane to catalysis is greater than that of (110) and (100), which influences the geometry of the crystal grain. After doping, the catalytic ability of all three phases improves, i.e., their adsorption energies tend toward that of Pt. Therefore, doping can

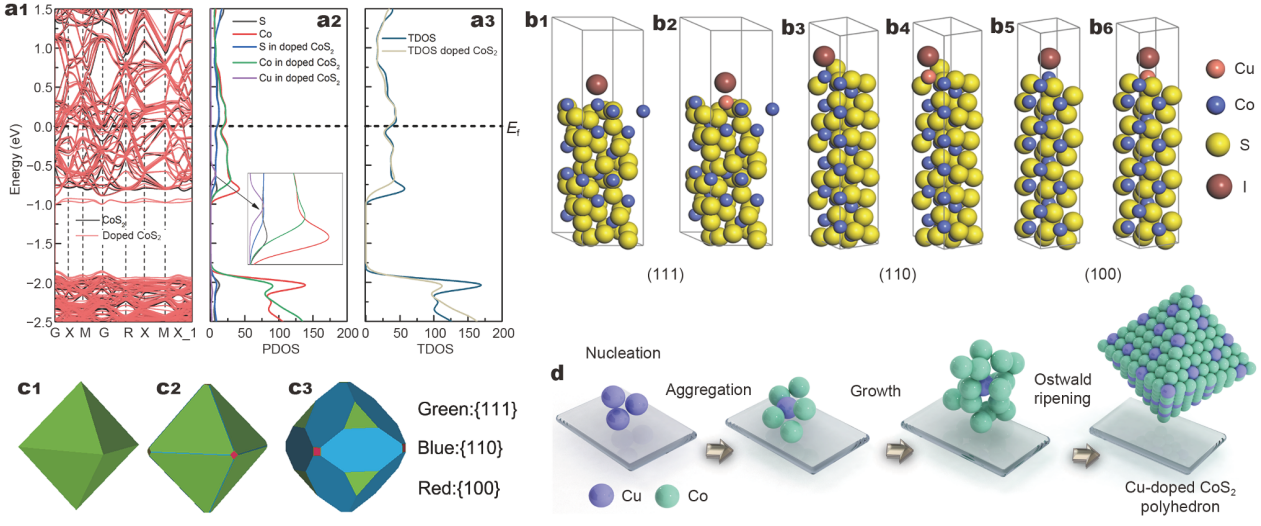

Figure 1 DFT calculations for CoS_2 before and after Cu doping: (a_1) band structure, (a_2) TDOS plots, and (a_3) PDOS plots of bulk CoS_2 and Cu-doped CoS_2, showing the bonding and antibonding states relative to the Fermi level. Slab models of bare CoS_2 with (b_1) (111), (b_3) (110) and (b_5) (100) surfaces. Iodine adsorbed on Cu-doped CoS_2 (b_2) (111), (b_4) (110) and (b_6) (100) surfaces. S: yellow, Co: blue, Cu: red, I: brown. Wulff prediction of crystal structures: (c_1) {111} pure surface, (c_2) {110} Cu-doped surface, (c_3) Cu over-doped {100} surface. Green: {111}, Blue: {110}, red: {100}. (d) Cu-doped CoS_2 growth on $TiCl_4$-treated FTO substrate.

simultaneously enhance the number and quality of the active crystals.

The effect of Cu doping on crystal planes' formation was also predicted by the surface energy calculations using the Wulff construction (Fig. 1c and Table S1). The surface energy is the most important thermodynamic parameter in crystal growth regulation. The values for the CoS_2 {111}, {110} and {100} planes are about 0.36, 1.12 and 1.48 J m^{-2}, indicating the thermodynamic stability is in the order of {111} > {110} > {100}. CoS_2 crystals can be theoretically modeled as a regular octahedron with eight equivalent {111} facets, but it is known that such crystals are subject to phase impurities, coalescence and aggregation that lead to irregular shapes. Thus, we analyzed the feasibility of controlling the tendency of crystal growth. The surface energies of the {111}, {110} and {100} planes on Cu-doped CoS_2 increased to 0.92, 1.25 and 2.41 J m^{-2}. In particular, the slight increase on {110} indicates that this plane can be easily grown with Cu doping. Meanwhile, it is difficult for the {111} and {100} planes to grow due to the increased surface energy (Table S2). Therefore, when doping with Cu, the truncated tetragonal bipyramidal shape of CoS_2 is transformed from an octahedron to polyhedron, which consists of twelve equivalent {110} planes, eight {111} planes, and six {100} planes. With the increase of the number of active crystal planes, the stability remains mostly unchanged, thus ensuring the long-term stability and highly efficient catalytic activity.

Catalyst loading on a conductive substrate is usually done to confer catalytic properties to a functional device. However, it is difficult to form CoS_2 particles directly on FTO substrates. Therefore, we used $TiCl_4$ to treat the FTO surface and enhance the lattice match degree, thus increasing the CoS_2 distribution density on the substrates. Table S3 shows the lattice constants of SnO_2, TiO_2 and CoS_2. When the polyhedron grows on bare FTO substrates, the distribution of CoS_2 is sparse due to the lack of effective growth sites. $TiCl_4$ pretreatment can accelerate the CoS_2 growth rate and increase its density on the substrate (Fig. 1d). This can be explained by the strong attraction beteween the Co^{2+} cationic precursor and oxygen-containing groups of the TiO_2 layer.

Then, Cu ions were introduced as nucleation seeds for crystal growth. The growing process was compared with that involving $TiCl_4$ pretreatment of the FTO surface (Fig. S1). With increasing $CuCl_2$, the particle size and morphology of precipitates vary greatly (Fig. S2). Large and irregular particles appear when no $CuCl_2$ is added. As the amount of $CuCl_2$ gradually increases, the irregular particles become smaller and more regular. The corresponding atomic percentages were estimated by the energy-dispersive X-ray spectroscopy (EDX). The Cu atomic ratio was 0.5%, 1.5%, 2.8% and 8.3%, respectively (Fig. S3). As seen in Fig. S4, for the Cu-0 sample, peaks were observed at 30.6°, 47.0°, and 32.3°, in addition to the characteristic diffraction peaks of FTO at 26.3°, 33.5°, 37.6°, 51.4°, 61.4°, and 65.3°. The detected peaks can be assigned to CoS (JCPDS 65-3418) and CoS_2 (JCPDS 41-1471), suggesting a low phase purity. However, better phase purity is observed for Cu-0.5, Cu-1.5 and Cu-2.8. The diffraction peaks at 27.9°, 32.3°, 36.2°, and 54.9° are well indexed to the (111), (200), (210), and (311) planes of CoS_2. No obvious peaks related to CoS are present. In Cu-8.3, a new peak emerges at 31.2°, which corresponds to (113) plane of $CuCo_2S_4$ (JCPDS 42-1450). This mixed crystal phase may be the cause of the irregular nanoparticles' shape.

Fig. S5 shows the time-dependent structure and distribution of the Cu-2.8 sample. The gradual growth of crystals, which corresponds to a typical hydrothermal growth process, is clearly observed. At the initial stage, Thioacetamide (TAA) decomposed into H_2S and then reacted with Cu^{2+} and Co^{2+} in the form of a complex. Small and irregular particles were formed and scattered on the FTO surface. Then, a mixture of polyhedrons and irregular-shaped CoS_2 of different sizes was observed. When the reaction time exceeded 10 h, the well-dispersed and well-formed polyhedrons grew much denser. The dense and uniform CoS_2 polyhedrons were well developed on FTO during a 20-h hydrothermal reaction. The formation mechanism of the polyhedrons corresponds to the Ostwald ripening process, where the growth velocity along the (100) direction was faster than that along the (111) direction, thus leading to the polyhedral structure. The particle size distribution of Cu-2.8 ranges from 380 to 480 nm (Fig. S6).

The scanning electron microscopy (SEM) micrographs show that Cu-doped CoS_2 with sharp conners and edges is evenly distributed on FTO, indicating the homogeneous dispersion of Cu, Co and S (Fig. 2a). The elemental ratio and particle size are consistent with the EDX results. Fig. 2b shows the transmission electron microscopy (TEM) and selected area electron diffraction (SAED) analysis of single crystal CoS_2. The diffraction spots have lattice spacings of 2.77, 2.27 and 1.85 Å, corresponding to the (200), (112) and (212) facets of CoS_2. Moreover, the lattice distances of 3.92, 3.22 and 2.49 Å can be ascribed to the (101), (111) and (210) planes of CoS_2, respectively. The angle between the (111) and (101)

facets is 90°, highly consistent with the theoretical value of cattierite CoS_2. The detected lattice distances were slightly enlarged compared with those reported for pure CoS_2 (3.91, 3.20 and 2.47 Å). This may be caused by the successful Cu doping because the ionic radius of Cu is larger than that of Co.

The effects of Cu doping on the surface states can be observed in the X-ray photoelectron spectroscopy (XPS): two peaks at 932.3 and 952.1 eV are assigned to the Cu $2p_{3/2}$ and $2p_{1/2}$ (Fig. 2c), respectively. The difference between the binding energies of these two peaks is 19.8 eV, implying a valence state of Cu^{+} [22,23]. The peaks at 933.8 and 954.3 eV are attributed to Cu^{2+}. The Co 2p spectra exhibit two doublets (Fig. 2d). The first doublet, at 778.8 and 793.9 eV, can be indexed to Co^{3+} $2p_{3/2}$ and Co^{3+} $2p_{1/2}$ electrons, agreeing with previous

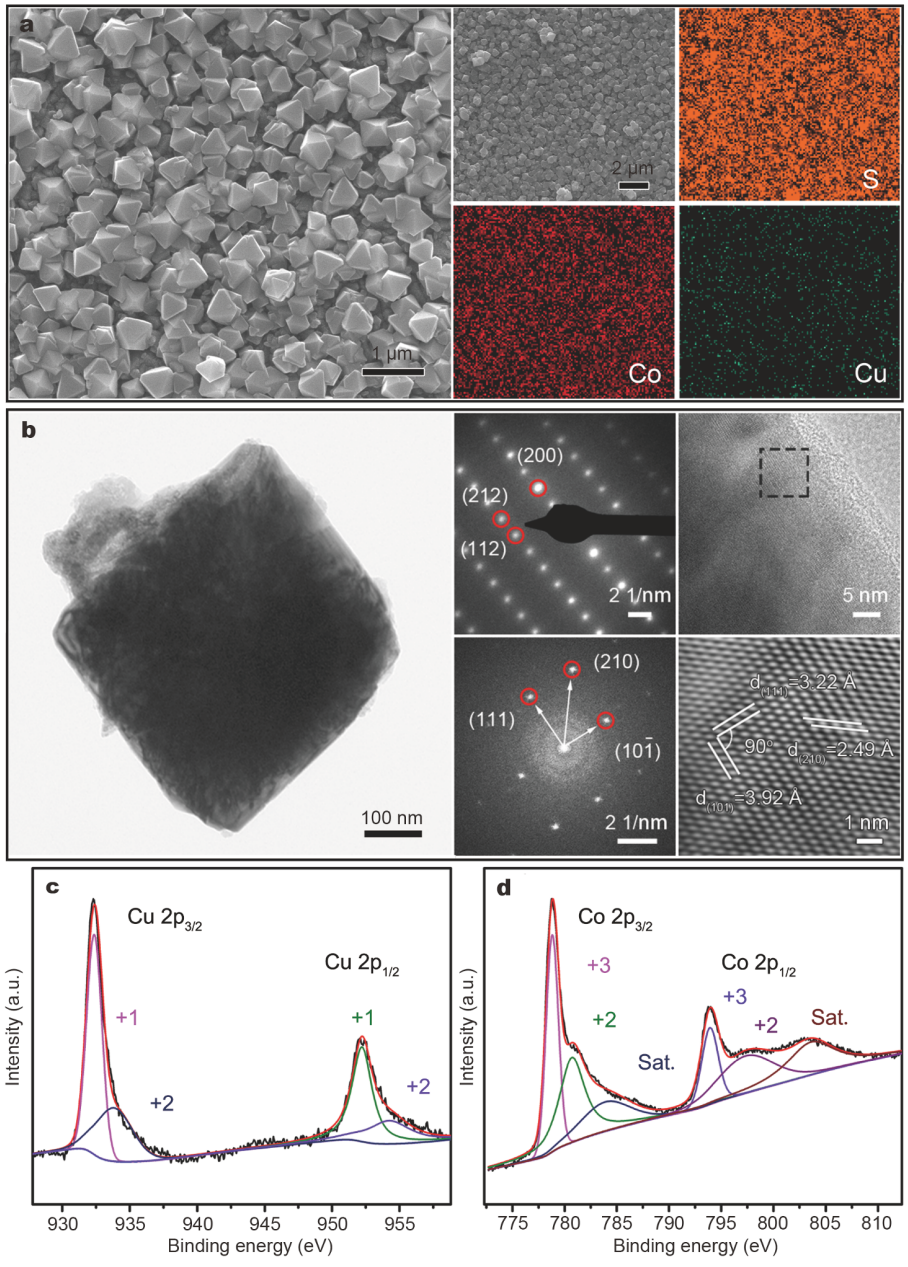

Figure 2 Characterizations of Cu-2.8. (a) SEM and EDX mapping; (b) TEM, high resolution TEM (HRTEM) and SAED pattern; and (c) Cu 2p and (d) Co 2p XPS spectra.

reports [20]. The second doublet, at 780.7 and 797.5 eV, correspond to Co^{2+} $2p_{3/2}$ and Co^{2+} $2p_{1/2}$ electrons. The difference between Co $2p_{3/2}$ and Co $2p_{1/2}$ is about 15.1 eV, confirming the coexistence of both Co^{3+} and Co^{2+} [24–26]. The S 2p spectrum shows peaks at 162.5, 163.6 and 168.9 eV that can be ascribed to the S $2p_{3/2}$ and S $2p_{1/2}$ electrons and a satellite peak, respectively (Fig. S7). Therefore, the surface of CoS_2 polyhedrons shows a variety of valence metals, including Cu^+, Cu^{2+}, Co^{3+}, Co^{2+}, and S^{2-}. Such variety of surface valences would likely contribute to the enhancement of the catalytic efficiency.

The catalytic reduction from I_3^- to I^- was selected as a model reaction to evaluate the electrocatalytic activity of the Cu-doped CoS_2 polyhedron/FTO system. Fig. 3a demonstrates that the short-circuit photocurrent density (J_{sc}) and photoelectric conversion efficiency (PCE) values increase and then decrease with increasing Cu as dopant. When the amount of Cu was small, the J_{sc} of the Cu-0.5 counter electrode (CE) decreased from 14.3 to 14.0 mA cm^{-2}. The poor crystallinity and low coverage on the FTO substrate led to a decrease in catalytic performance and in the J_{sc}. When further increasing the content of Cu, the PCE of Cu-1.5 and Cu-2.8 CEs reached 7.02% and 7.34%, respectively, which are close to the value of conventional sputtered Pt CEs (7.37%). The enhancement of the PCE and J_{sc} values of Cu-2.8 CE are mainly ascribed to the optimized absorption energies on both {111} and {110} planes, which leads to an accelerated adsorption/desorption process of the I^-/I_3^- couple. The over-doped Cu-8.3 CE suffered from a remarkable decline in PCE, 4.93%, caused by the poor morphological and structural properties mentioned above. The photovoltaic performances are listed in Table S4. The high and low J_{sc} values can be further explained in terms of the electrochemical properties of the CEs. Based on the cathodic peak current density (J_{cp}) and peak-to-peak separation (E_{pp}), the two pairs of redox peaks imply a good electrocatalytic ability of the Cu-doped CoS_2 polyhedron CEs (Fig. 3b). The Cu-0 CE exhibited the same E_{pp} (0.32 V) as that of a Pt CE, indicating the fast electron transfer at the electrode interface. The E_{pp} value of the Cu-2.8 (0.28 V) CE was smaller than that of Cu-0, indicating an enhanced conductivity. In addition, the J_{cp} values were as follows; Pt (1.53 mA cm^{-2}) < Cu-0.5 (1.73 mA cm^{-2}) < Cu-1.5 (1.75 mA cm^{-2}) < Cu-2.8 (1.86 mA cm^{-2}) (Table 1). These results indicate that Cu doping actually enhances the catalytic active sites. The changes in current density and electrochemical impedance were monitored to evaluate the catalytic activity. The exchange current density (J_0) and limiting diffusion current density (J_{lim}) were evaluated to investigate the reaction kinetics (Fig. 3c). The Cu-2.8 CE reached a higher J_{lim} (60.3 mA cm^{-2}) than a Pt

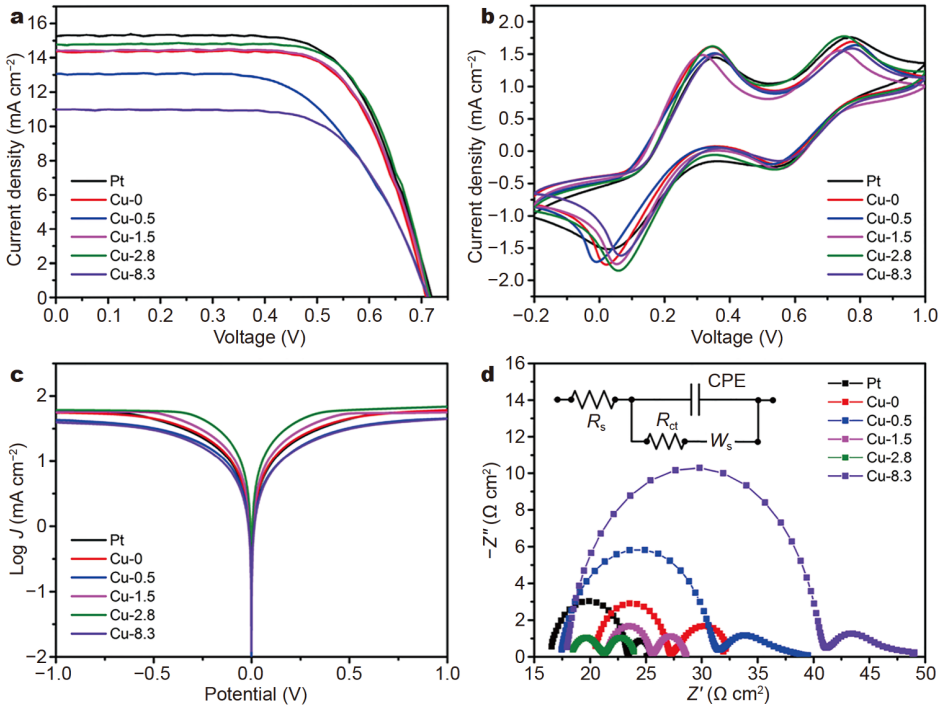

Figure 3 (a) Photocurrent density-voltage (*J-V*), (b) CV, (c) Tafel polarization and (d) Nyquist plots with the equivalent circuit model.

Table 1 The parameters of Pt, Cu-0, Cu-0.5, Cu-1.5, Cu-2.8 and Cu-8.3

Sample	E_{pp} (V)	J_{cp} (mA cm^{-2})	J_{lim} (mA cm^{-2})	J_0 (mA cm^{-2})	R_s (Ω cm^2)	R_{ct} (Ω cm^2)	CPE (μF cm^{-2})	W_s (Ω cm^2)
Pt	0.32	1.53	54.9	6.76	16.4	6.86	7.76	2.03
Cu-0	0.32	1.75	56.2	7.07	20.4	6.67	3.18	5.14
Cu-0.5	0.35	1.73	42.6	5.88	17.4	13.4	11.7	7.43
Cu-1.5	0.26	1.75	57.5	8.71	21.5	3.91	15.7	3.13
Cu-2.8	0.28	1.86	60.3	13.5	18.3	2.77	39.3	2.91
Cu-8.3	0.35	1.63	38.9	4.78	17.9	7.34	22.7	2.26

CE (54.9 mA cm^{-2}). Since J_{lim} determines the ionic diffusion coefficient, a higher J_{lim} indicates a faster diffusion of the I^-/I_3^- couple. The relationship between J_0 and the charge transfer resistance (R_{ct}) is $J_0=RT/nFR_{ct}$, where R is the gas constant, T is the absolute temperature, F is the Faraday's constant, n is the number of electrons involved in the reduction reaction. The J_0 values were: Cu-8.3 (0.68 mA cm^{-2}) < Cu-0.5 (0.77 mA cm^{-2}) < Cu-0 (0.85 mA cm^{-2}) < Cu-1.5 (0.94 mA cm^{-2}) < Cu-2.8 (1.13 mA cm^{-2}), demonstrating the best catalytic activity would be for Cu-2.8. Moreover, Cu-2.8 CE displayed a higher J_0 than the Pt CEs, which indicates a higher electron transfer capability for the Cu-doped CoS_2 polyhedrons. The interfacial electron transfer process was analyzed by electrochemical impedance spectrum (EIS) (Fig. 3d). The evaluated parameters included the charge transfer resistance (R_{ct}), series resistance (R_s) and Warburg diffusion resistance (W_s) in different frequency regions. A small R_s value of 18.3 Ω cm^2 was achieved by the symmetrical Cu-2.8 CE, and was similar to that of the Pt CE (16.4 Ω cm^2), possibly due to the strong interaction with the substrate. Such low R_s value would favor the electron migration at the CoS_2/FTO interface, thus improving the J_{sc} and fill factor (FF). It is worth noting that the Cu-2.8 CE has the largest constant phase element (CPE), which can be attributed to the reduced particle size that increases the catalytic surface area. In addition, the Cu-2.8 CE displayed a lower R_{ct} (2.77 Ω cm^2) than the Pt (6.88 Ω cm^2) and Cu-0 (6.86 Ω cm^2) electrodes, indicating the Cu dopant can reduce the R_{ct} and improve the electrical conductivity of CoS_2. The low impedance characteristics may lead to a highly efficient electron transfer in the reaction, thereby improving the catalytic efficiency. These observations were consistent with the DFT results; the Cu-doped CoS_2 polyhedrons exhibited an accelerated electron transfer at the electrode/electrolyte interface, and also an improved I_3^- catalytic reduction.

The long-term durability of the catalysts was estimated by successive cyclic voltammetry (CV) and EIS measurements in a highly corrosive iodine electrolyte. After 120 CV scans, the plot geometry and peak current size were almost unchanged (Fig. 4a). For Cu-2.8 CE, the values of R_{ct}, R_s and W_s remain almost the same, whereas for Pt, R_{ct} increases from 6.88 to 10.5 Ω after 10 cycles (Fig. 4b and c). The stability of Cu-2.8 can be ascribed to its ultra-stable single crystalline nature and high resistance to chemical corrosion.

In summary, when CoS_2 is doped with Cu, the number of active crystal planes is effectively increased and the relative stability of the crystal planes is improved. The crystal plane synergy is mainly evidenced in the crystal

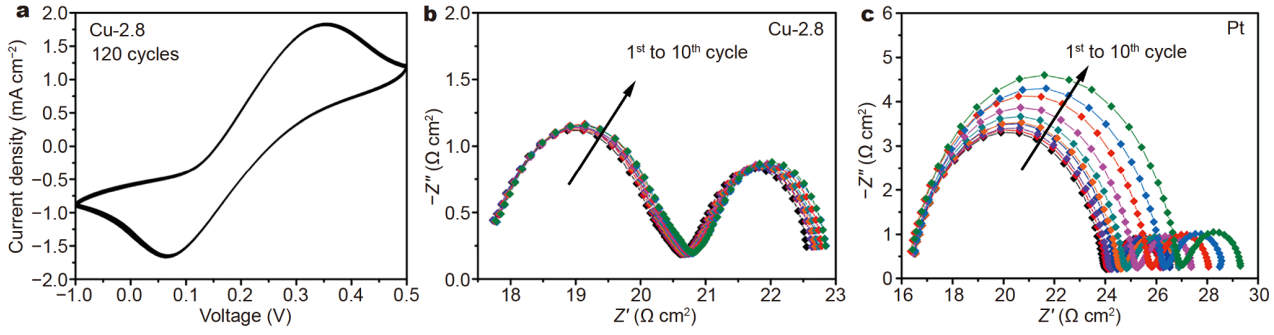

Figure 4 (a) Successive CV curves of Cu-2.8 CEs at a scan rate of 50 mV s^{-1}. Repeated EIS curves of (b) Cu-2.8 and (c) Pt CEs in acetonitrile solution. EIS: 10 cycles, ranging from 10^5 to 0.1 Hz.

growth and electron transfer processes. The number and stability of active crystal planes can ensure a highly efficient and stable catalytic activity. Moreover, the absorption energies of the (111), (110), and (100) facets can be optimized to −2.00, −1.52, and −3.13 eV, respectively, due to the accelerated adsorption/desorption of the I^-/I_3^- couple. A high PCE of 7.34% was achieved with dye-sensitized solar cells based on the Cu-doped-CoS_2 CEs, which is comparable to the value obtained with Pt (7.37%). The results of this work provide an interesting approach for designing and preparing high-performance non-precious metal catalysts in large-scale.

Received 9 January 2020; accepted 24 March 2020; published online 28 April 2020

1 Li X, Zhang W, Cai J, *et al.* Hierarchical nanosheets constructed by integration of bimetallic sulfides into N-doped carbon: Enhanced diffusion kinetics and cycling stability for sodium storage. Nano Energy, 2019, 62: 239–249
2 Xiao Y, Zhou M, Liu J, *et al.* Phase engineering of two-dimensional transition metal dichalcogenides. Sci China Mater, 2019, 62: 759–775
3 Dong F, Guo Y, Xu P, *et al.* Hydrothermal growth of MoS_2/Co_3S_4 composites as efficient Pt-free counter electrodes for dye-sensitized solar cells. Sci China Mater, 2017, 60: 295–303
4 Wang W, Wang Y, Li C, *et al.* Design, synthesis and electrocatalytic properties of coaxial and layer-tunable MoS_2 nanofragments/TiO_2 nanorod arrays. Chem Commun, 2017, 53: 5461–5464
5 Wang W, Bi H, Li C, *et al.* Edge-terminated few-layer MoS_2 nanoflakes supported on TNAs@C with enhanced electrocatalysis activity for iodine reduction reaction. Mater Today Nano, 2019, 6: 100033
6 Zhao Y, Song B, Cui X, *et al.* High electrocatalytic reduction using ZnS micropolyhedron: Direct sulfuration of ZIF-8 film on conducting glass by chemical vapour deposition. Mater Lett, 2019, 250: 193–196
7 Wang Y, Bai Y, Xi J, *et al.* Continuous and large-area transition metal disulfides films deposited by pulsed laser/chemical vapor-combined process as a counter electrode for dye-sensitized solar cells. Mater Lett, 2017, 201: 216–220
8 Liu Y, Yin J, Zhou Y, *et al.* Tuning electron transport direction through the deposition sequence of MoS_2 and WS_2 on fluorine-doped tin oxide for improved electrocatalytic reduction efficiency. ChemElectroChem, 2019, 6: 2737–2740
9 Shi Y, Zhou Y, Yang DR, *et al.* Energy level engineering of MoS_2 by transition-metal doping for accelerating hydrogen evolution reaction. J Am Chem Soc, 2017, 139: 15479–15485
10 Feng JX, Wu JQ, Tong YX, *et al.* Efficient hydrogen evolution on Cu nanodots-decorated Ni_3S_2 nanotubes by optimizing atomic hydrogen adsorption and desorption. J Am Chem Soc, 2018, 140: 610–617
11 Yin J, Jin J, Zhang H, *et al.* Atomic arrangement in metal-doped NiS_2 boosts the hydrogen evolution reaction in alkaline media. Angew Chem Int Ed, 2019, 58: 18676–18682
12 Shen L, Wang Y, Wu F, *et al.* Hierarchical metal sulfide/carbon spheres: A generalized synthesis and high sodium-storage performance. Angew Chem Int Ed, 2019, 58: 7238–7243
13 Xue S, Chen L, Liu Z, *et al.* $NiPS_3$ nanosheet–graphene composites as highly efficient electrocatalysts for oxygen evolution reaction. ACS Nano, 2018, 12: 5297–5305
14 Yu C, Liu Z, Chen Y, *et al.* CoS nanosheets-coupled graphene quantum dots architectures as a binder-free counter electrode for high-performance DSSCs. Sci China Mater, 2016, 59: 104–111
15 Han X, Wu X, Deng Y, *et al.* Ultrafine Pt nanoparticle-decorated pyrite-type CoS_2 nanosheet arrays coated on carbon cloth as a bifunctional electrode for overall water splitting. Adv Energy Mater, 2018, 8: 1800935
16 Zheng J, Zhou W, Ma Y, *et al.* Facet-dependent NiS_2 polyhedrons on counter electrodes for dye-sensitized solar cells. Chem Commun, 2015, 51: 12863–12866
17 Zheng J, Guo Z, Zhou W, *et al.* Synergistic effect of Ni and Fe in Fe-doped NiS_2 counter electrode for dye-sensitized solar cells: Experimental and DFT studies. Electrochim Acta, 2018, 284: 24–29
18 Wang J, Wang J, Han L, *et al.* Fabrication of an anode composed of a N, S co-doped carbon nanotube hollow architecture with CoS_2 confined within: toward Li and Na storage. Nanoscale, 2019, 11: 20996–21007
19 Qu G, Wu T, Yu Y, *et al.* Rational design of phosphorus-doped cobalt sulfides electrocatalysts for hydrogen evolution. Nano Res, 2019, 12: 2960–2965
20 Zhang J, Xiao B, Liu X, *et al.* Copper dopants improved the hydrogen evolution activity of earth-abundant cobalt pyrite catalysts by activating the electrocatalytically inert sulfur sites. J Mater Chem A, 2017, 5: 17601–17608
21 Hou Y, Wang D, Yang XH, *et al.* Rational screening low-cost counter electrodes for dye-sensitized solar cells. Nat Commun, 2013, 4: 1583
22 Chauhan M, Reddy KP, Gopinath CS, *et al.* Copper cobalt sulfide nanosheets realizing a promising electrocatalytic oxygen evolution reaction. ACS Catal, 2017, 7: 5871–5879
23 Liu S, Yin Y, Hui KS, *et al.* High-performance flexible quasi-solid-state supercapacitors realized by molybdenum dioxide@nitrogen-doped carbon and copper cobalt sulfide tubular nanostructures. Adv Sci, 2018, 5: 1800733
24 Zhu J, Tang S, Wu J, *et al.* Wearable high-performance supercapacitors based on silver-sputtered textiles with $FeCo_2S_4$-$NiCo_2S_4$ composite nanotube-built multitripod architectures as advanced flexible electrodes. Adv Energy Mater, 2017, 7: 1601234
25 Zhang X, Su D, Wu A, *et al.* Porous NiCoP nanowalls as promising electrode with high-area and mass capacitance for supercapacitors. Sci China Mater, 2019, 62: 1115–1126
26 Liu W, Zhang J, Bai Z, *et al.* Controllable urchin-like $NiCo_2S_4$ microsphere synergized with sulfur-doped graphene as bifunctional catalyst for superior rechargeable Zn-air battery. Adv Funct Mater, 2018, 28: 1706675

Acknowledgements We acknowledge the funding support from the National Natural Science Foundation of China (61774033) and Guangdong Province Key Area R&D Program (2019B010940001).

Author contributions Yin J performed the experiments and characterizations with the help of Lu M and Song L, Chen P performed the calculations with support of Wu N. Yin J, Chen P and Lu M contributed equally to this work. Zhang R and Xu F contributed to data analysis and interpretation. Wang Y conceived the idea, wrote the paper, supervised all students and acquired the funding. All authors have approved the manuscript for publication.

Conflict of interest The authors declare that they have no conflict of interest.

Supplementary information Experimental details and supporting data are available in the online version of this manuscript.

Jie Yin is currently a PhD candidate in Nano Photo-electrochemistry & Device Group at the Southeast University, under the supervision of Prof. Yuqiao Wang. He received his BS degree in Chemical Engineering and Technology from Kunming University of Science and Technology in 2012. His research interests focus on the synthesis and electro-catalytic mechanism of the multi-metal chalcogenides.

Pin Chen received his BS degree in Anqing Normal University in 2011 and MS degree from South China University of Technology in 2014 under the supervision of Prof. Yan Mu. Currently, he is a high-performance computing engineer at the National Supercomputer in Guangzhou Center (NSCC-GZ). His interests focus on high-performance parallel computing and multi-scale material calculation.

Minglong Lu is currently a Master candidate in Nano Photo-electrochemistry & Device Group at the Southeast University, under the supervision of Prof. Yuqiao Wang. He received his BS degree in materials chemistry in 2018 from Nanjing University of Science and Technology. His current research focuses on the development of high-efficiency catalysts for photo-electrochemical cells.

Yuqiao Wang received his BS in fine chemicals from Anhui University, and MS and PhD in material physics & chemistry from Southeast University. Now, he is a Full Professor at Southeast University, and the Head of Nano Photoelectrochemistry & Device Lab. His current research interests include the design and synthesis of nanostructured photoelectric functional materials, the related photoelectric device integration, and the relationship between material invalidation and device performance attenuation.

具有高催化活性和长期稳定性的铜掺杂CoS_2多面体

印杰[1†], 陈品[2†], 卢明龙[1†], 宋利黎[1], 张仁云[3], 徐峰[4], 吴宁宁[2], 王育乔[1*]

摘要 过渡金属硫化物作为贵金属的替代材料具有成本低和催化活性高的特点. 本文中, 我们提出了一种直接在导电玻璃上可控生长Cu掺杂CoS_2多面体的方法, 并通过调节活性晶面的分布和数量使其具有高催化活性和稳定性. 铜掺杂后, CoS_2的表面结构可以由无序的纳米粒子转变为多面体, 包含12个{110}, 8个{111}和6个{100}晶面. 活性晶面的数目和稳定性由此得到改善, 并且对I_3^-离子的还原反应表现出了高效而稳定的催化活性. 我们利用Wulff构筑法和第一性原理计算研究了铜掺杂CoS_2多面体的生长机理和催化过程. 结果表明, Cu(0.5 At.%)掺杂后, CoS_2样品的电荷转移速率、吸脱附I原子的能力和稳定性均得到增强, 其催化性能可以和Pt媲美.

